Asian Journal of Chemistry; Vol. 32, No. 11 (2020), 2722-2730

ASIAN JOURNAL OF CHEMISTRY

https://doi.org/10.14233/ajchem.2020.22803

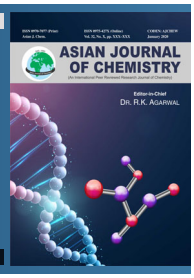

Enhancement Supercapcitive Behaviour of Cobalt(II) Tetrasulfanilamide Phthalocyanine with Composite rGO on Modified GCE

K.R. Venugopala Reddy[1,*], N.Y. Praveenkumar[1], Mounesh[1], T.M. Sharanakumar[2] and Sangappa K. Ganiger[3]

[1]Department of Studies and Research in Chemistry, Vijayanagara Sri Krishnadevaraya University, Ballari-583105, India
[2]Ballari Institute of Technology and Management, Ballari-583104, India
[3]Department of Physics, Government Engineering College, Raichur-584134, India

*Corresponding author: E-mail: venurashmi30@gmail.com

Received: 14 January 2020; *Accepted*: 5 April 2020; *Published online*: 28 October 2020; AJC-20093

A novel method for the fabrication of tetrasulfanilamide cobalt(II) phthalocyanine (CoTSPC) was developed and the synthesized product was characterized using various techniques namely UV-visible, infrared and X-ray diffraction spectroscopic and thermal gravimetric analysis. An electrode with glassy carbon was modified on CoTSPC with an rGO composite. The effect of experimental parameters, such as precipitation agent, precursor concentration, reaction time and stabilizing agent, was systematically studied to investigate possible CoTSPC formation. The electrochemical properties of prepared CoTSPC/rGO/GCE were explored through cyclic voltammetry (CV) by using a three-electrode system. The results showed that the specific capacitances and sizes of the fabricated compounds are related. Due to a large surface area, within an operated voltage range of –0.2 to 0.4 V, synthesized CoTSPC/rGO/GCE exhibited an excellent long-cycle life and the highest capacitance (157 F g^{-1}), thereby indicating that fabricated CoTSPC/rGO/GCE can be used as an outstanding electrode material in supercapacitors.

Keywords: Amino acid, Ultrasound, Aqueous media, Cavitation.

INTRODUCTION

Due to potential physical and chemical properties, which are induced by macromolecular structure of metal phthalocyanines (MPcs), they have received considerable attention. Metal phthalocyanines (MPcs) have highly delocalized electrons; 18 π-electrons are present in an MPc macrocycle, and can exhibit the conductivity through electron delocalization [1]. They have received substantial attention for device upgrade, due to their electronic properties and efficiency in converting energies, and present a potential for applications in switching devices [2,3]. In a metal-phthalocyanine molecule, a π-conjugated ligand bonded to the central metal atom. Metal phthalocyanine molecules can exhibit conducting, semiconducting properties and are employed in intrinsic semiconductors [4]. In electrochemical supercapacitors, the energy density is lower than that in storage devices and power density shows the order of the storage units of primary energy [5-7]. Porous structures, such as graphite nanofibres, activated carbons and carbon nanotubes, were employed as possible materials to study the behaviour of supercapacitors [8-10]. Graphene and metal phthalocyanine were used to combine the semiconducting and monomolecular sheet properties of tetracarboxy cobalt(II) phthalocyanine (CoTCPc) and graphene oxide (GO) for charge transfer, which resulted in the novel applications of carbon nanotubes and GO-doped CoTCPc films, which is the major benefit of selecting highly mobile MPcs as active layers to develop next-generation electronic devices [11].

Molecules with -NH groups exhibit supercapacitance. In this study, we synthesized phthalocyanine with a -NH group. Moreover, nanocomposites, nanomaterials, and active carbon materials can improve the supercapacitance of molecules. These molecules have porous structures, which increases their surface area for charge transfer. Therefore, we mixed active carbon materials such as graphene with metal phthalo-cyanine. The molecules were studied through CV. In CV studies, cyclic voltammogramms are acquired at different scan rates, and then are compared.

In this study, a one-step method is established to synthesize CoTSPC/rGO/GCE composites. Under mild conditions, CoTSPC/GC electrodes grow on rGO sheets. The proposed method is environmentally friendly, simple and abundant in materials and can yield CoTSPC/rGO/GCE composites having outstanding cycling stability, which is beneficial for supercapacitors and high specific capacitance.

EXPERIMENTAL

Trimellitic anhydride, sulfanilic acid, reduced graphene oxide (rGO) purchased from Sigma-Aldrich, USA.The solvents *viz*. sodium hydroxide, hydrochloric acid, urea, cobalt chloride, dimethyl formamide, *N*,*N*′-dicyclohexylcarbodiimide (DCC) were purchased from Spectrochem chemicals.

Synthesis of tetracarboxy cobalt phthalocyanine: CoTCPc was synthesized by a slight modification of the procedure reported in the literature [12]. The finely grounded mixture of trimellitic anhydride (0.4 mmol), urea (0.1 mol), catalytic quantity of ammonium molybdate (0.4 mmol) and $CoCl_2$ (0.1 mmol) was charged into 25 mL of DMSO and refluxed for 4 h at 180 ºC (**Scheme-I**). A dark green coloured complex was washed with ethanol followed by 0.5 mol L^{-1} of HCl, 0.5 mol L^{-1} NaOH in combination with saturated NaCl solutions. Finally, the crude product was thoroughly washed with distilled water until free from acid and dried over P_2O_5 in a vacuum desiccator. Yield: 75 % Anal. for CoTCPc, m.w. 684.46; $C_{36}H_{17}O_8N_6Co$, calcd. (found) (%): C 57.9 (57.10); H 2.50 (2.42); N 12.27 (12.20); O 18.70 (18.65); Co 8.61 (8.60).

Synthesis of cobalt(II) tetrasulfanilamidephthalocyanines (CoTSPC): CoTSPC was synthesized according to the procedure described earlier [12-15]. In dry clean round bottom flask, 25 mL of DMF was mixed with CoTCPc (9×10^{-4} mmol) and K_2CO_3 (9×10^{-4} mmol) and stirred constantly for 30 min. A catalytic amount of *N*,*N*′-DCC then added along with sulfanilic acid (4×10^{-4} mmol) with constant stirring for 48 h yields a dark green coloured product (**Scheme-II**). The product was separated by filtration followed by the successive washing with excess of hot water and then with *n*-hexane. The obtained product was dried using P_2O_5 in desiccator. Yield: 81%. Anal. for CoTSPC with m.w. 1220; $C_{56}H_{21}O_{16}N_6S_4Co$; calcd. (found) (%): C 55.00 (54.51), H 1.71 (1.57), O 21.00 (20.91), N 6.88 (6.80), S 10.51 (10.25), Co 4.82 (4.72); UV-vis (H_2SO_4) λ_{max}

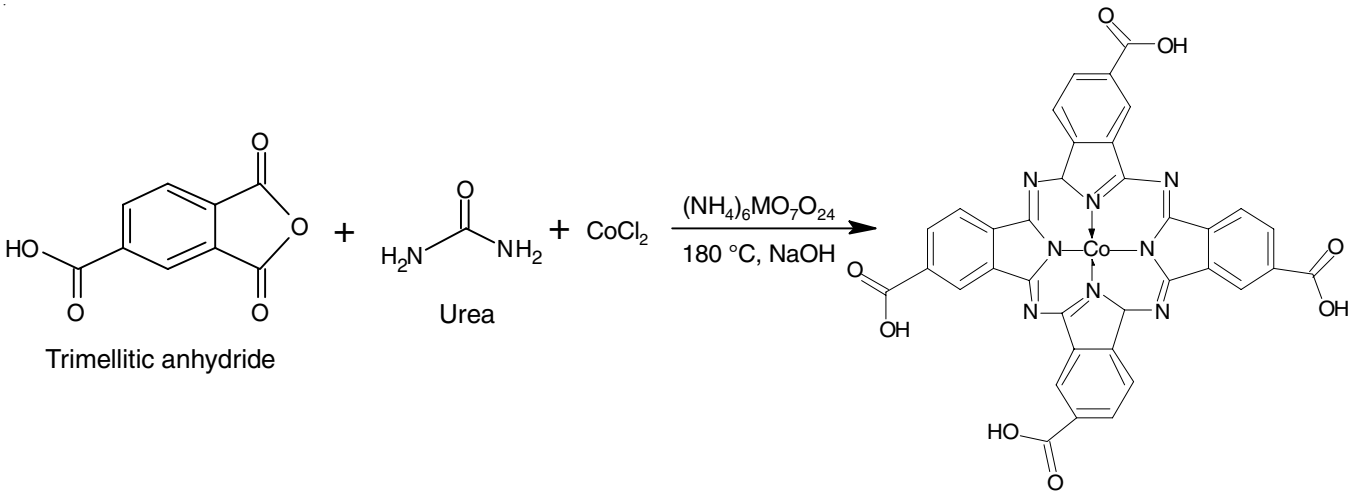

Scheme-I: Synthesis of tetra-carboxylic acid cobalt(II) phthalocyanine (CoTCPc)

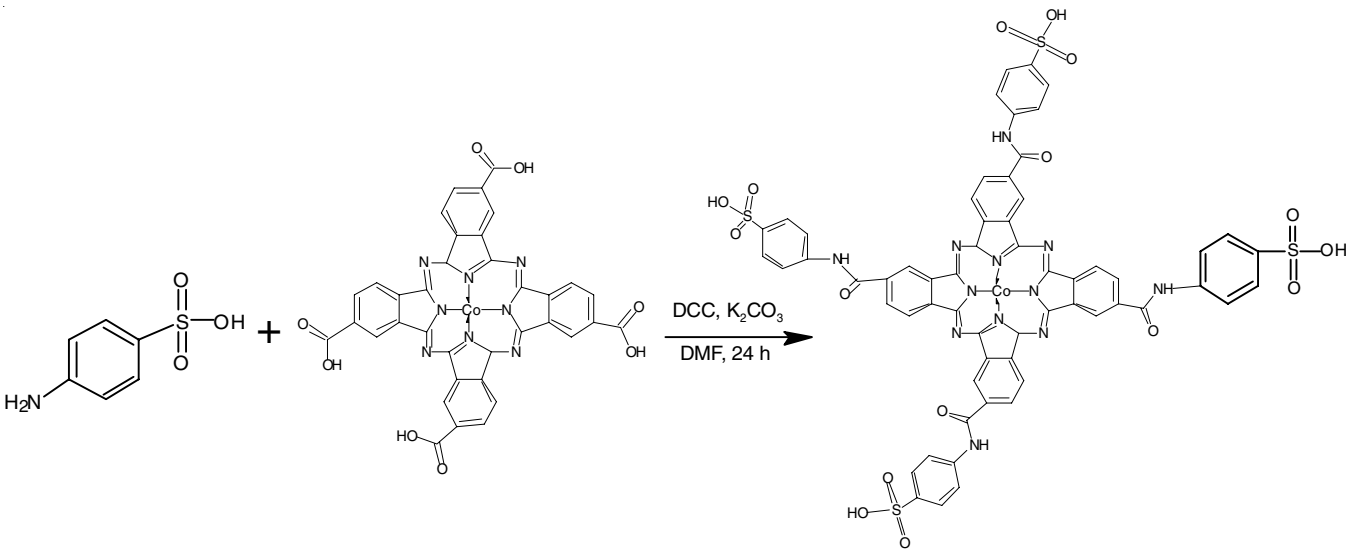

Scheme-II: Synthesis of tetra-sulfanilamide cobalt(II) phthalocyanine (CoTSPc)

(nm): 333, 430, 607, 619. IR absorption bands (KBr, ν_{max}, cm^{-1}): 3340, 1668, 1640, 1510, 1415, 1391, 1319, 1279, 1232, 1168, 1148, 1103, 1067, 937, 842, 765.

Preparation of modified electrodes: The CoTSPC/rGO/GCE composites were prepared by one step method. In a typical procedure, 0.05 g of CoTSPC was dissolved in 5 mL of dry DMSO and different weight of rGO suspension solution (5, 10, 15 and 20 mg) followed by the addition of 10 mL of DMSO. The resulting solution was stirred for 30 min at room temperature and refluxed at 60 ºC for 3 h. After the reaction finished, the solution was allowed to cool at room temperature and the resulting product was separated by filtration, washed with distilled water and then ethanol several times. For analysis, pure rGO was obtained by using 1M sulfuric acid to deal with the resultant composites to formation of CoTSPC/rGO/GCE. This electrode was used for study the supercapacitance behaviour by electrochemical measurements in cyclic voltammeter.

Characterization: The absorption spectra were recorded by using instrument Shimadzu UV-550 spectrophotometer. The IR analysis was conducted in the region of 4000-500 cm^{-1} using Perkin Elmer Spectrum 100 FT-IR spectrophotometer. The XRD analysis was performed on BRUKER Advanced D8 spectrophotometer Cu-Kα radiation source. Thermogravimetric analysis was performed on a Mettler Toledo instrument with a heating rate of 20 ºC/min and a nitrogen flow rate of 50 mL/min.

The electrochemical measurements were performe on the CHI620 Electrochemical workstation, USA, provided with three electrodes containing 1 M H_2SO_4 as electrolyte. Here three electrodes were GCE, platinum electrode as a counter electrode and Ag/AgCl electrode reference electrode. And GCE as working electrode was modified with the GO and GO-CoTSPC using drop deposition method. The capacitance can be measured in low concentration of electrolyte as 1 M H_2SO_4.

RESULTS AND DISCUSSION

UV-visible studies: For optical characterization, the synthesized CoTSPc-GO and CoTsPc composites were dispersed into the DMF solvent. Fig. 1 illustrates the UV-vis spectra for dispersion. The CoTSPc spectrum showed two characteristic bands of absorption peaks; B and Q bands appeared at 273-350 and 750 nm, respectively, due to deep p level and π-π* transition, respectively (Fig. 1a and b). Electronic transitions between molecular orbitals resulted from HOMO and LUMO correspond to π-π* transition states [16,17]. In CoTSPC-GO, an additional peak near 220 nm accompanied with B and Q bands. This peak was caused by the π-π* transition of the sp^2 hybridized GO carbon network. Optical spectra indicated the generation of CoTSPc and its composites (Fig. 1b).

FTIR studies: In IR spectra, a new broad peak observed in the 3600-3200 cm^{-1} range for -COOH (Fig. 2c) of CoTCPc disappeared, while a new peak appeared at 3330 cm^{-1} correspond to -CONH group (Fig. 2a) and a rGO/CoTSPC peak appeared at 3600-3200 cm^{-1} (Fig. 2b), confirmed the compound formation. A band corresponding to Ar-CH appeared in the range of 3067-2931 cm^{-1}; sharp peaks for the stretching vibrations of ν(C=C) and ν(C=N) groups appeared near 1496-1467 and

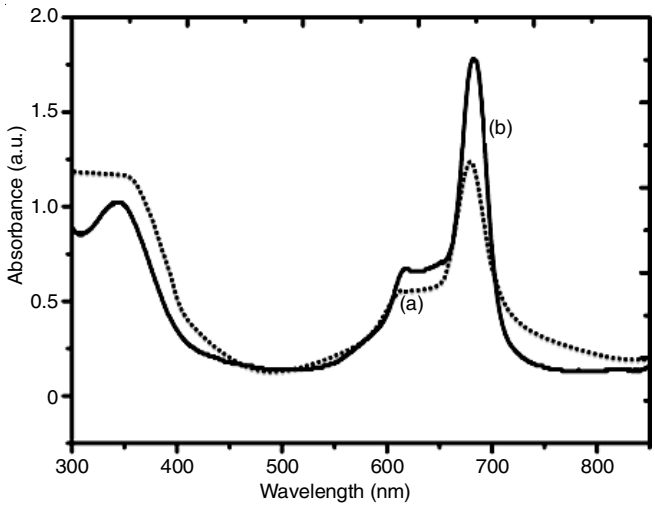

Fig. 1. UV-vis spectra of (a) CoTSPC and (b) CoTCPC

1724-1615 cm^{-1} ν(C=N; C=O); a sharp peak appeared at 1388 for the C-C group; and a sharp peak corresponding to C-Br was observed at 749. The Peaks appearing at 1226, 1283, 1118, 1154, 932, 1071, 638, 848, 543, 578 and 459 cm^{-1} (Fig. 2c-b) were attributed to the different skeletal vibrations of CoTCPC and CoTSPC rings. The IR spectral data supported proposed target structures.

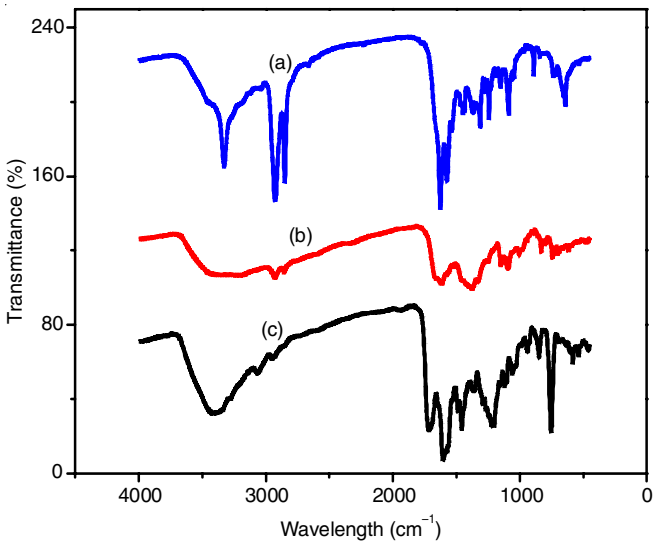

Fig. 2. FTIR spectra of (a) CoTCPC, (b) CoTSPC and (c) CoTSPC/rGO

Elemental analysis: For hydrogen, carbon and nitrogen, elemental analysis was performed using the Vario EL III CHNS analyzer. To estimate metal contents present in CoTSPc and CoTCPc, a known amount of complexes was decomposed by employing a mixture of H_2SO_4 and HNO_3, and then the resulting product was carefully evaporated and calcinated [18,19].

XRD studies: XRD was used to analyze the crystal structures of the samples. Fig. 3 presents the XRD patterns of CoTSPc and CoTCPc with GO composites. The three sharp diffraction peaks obtained for CoTSPc at the 2θ of 40.24º, 52.74º and 69.42º, which correspond to (111), (200) and (220) reflections, respectively, were attributable to cobalt. Two sharp diffraction peaks observed for CoTSPC at the 2θ of 40.45º and 72.37º

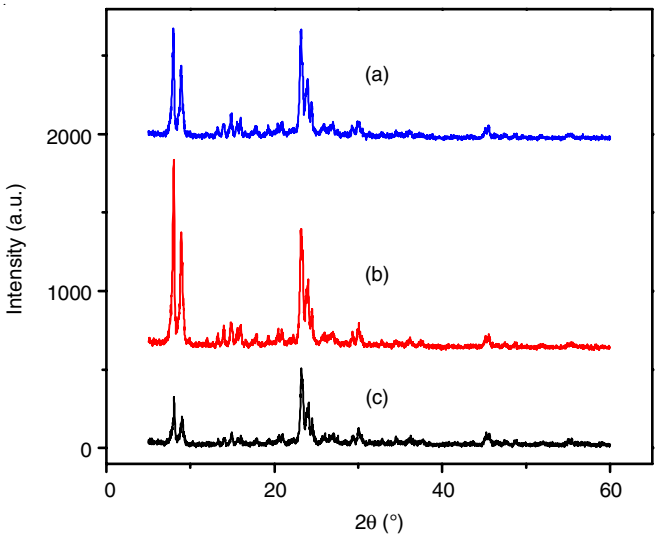

Fig. 3. XRD spectra of (a) CoTCPC, (b) CoTSPC and (c) CoTSPC/rGO

correspond to (111) and (220) planes of cobalt. CoTSPC was doped on GO, thus CoTSPC with GO exhibited a sharp graphite peak, corresponding to the (002) reflection, at 2θ of 26º. This peak indicated that the synthesised complexes had a crystalline structure. Moreover, in the presence of GO, the degree of graphitization of CoTSPC increased. Thus, the capacitance behaviour of CoTSPC having GO substantially changed.

Thermal studies: Thermal studies facilitated the understanding of macromolecule (phthalocyanine) decomposition and the thermal stability of CoTSPc/GO and CoTSPc complexes for different ranges of temperature. TGA curves confirmed that in the air atmosphere, the complexes underwent decomposition in three main steps (Fig. 4). In the first stage below 205 ºC, mass loss occurred through the decomposition of volatile substances and water was eliminated as moisture from the sample through exothermic decomposition. In the second stage, the substituents of the carboxylic group decomposed at 350-450 ºC. The third stage occurred readily in an oxidizing atmosphere, and in this stage, weight loss accelerated in accordance with the phthalocyanine structure decomposition after 530 ºC. In the oxidizing atmosphere, the steady formation of final products from complexes was equivalent to the cobalt oxide (CoO) mass

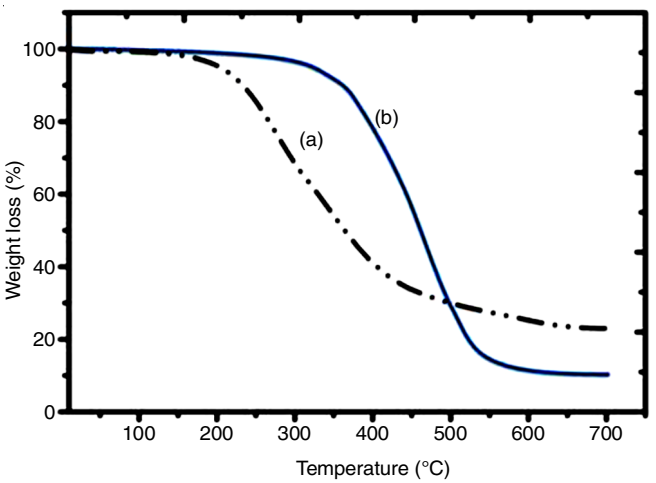

Fig. 4. Thermogravimetric analysis of (a) CoTSPC and (b) CoTSPC/rGO

[20]. In the final stage, cobalt underwent oxidation to produce cobalt oxide [15]. This finding indicated complexes having high purity, which was revealed from the elemental analysis data of the complexes [22-24].

Cyclic voltammetry: For all the molecules having a nitrogen group, ions may have a sufficient time and low probability to diffuse onto the electrode surface at lower and higher discharge current rates, respectively [21,22]. Moreover, graphene oxides, active carbon materials and carbon nanotubes have a large surface area [24] and numerous porous structures [23]. When these materials are doped with other molecules having a small surface area, their surface area increases, which improves in their activities [25]. These results are considerably helpful for electrodes with a larger amount of rGO because these electrodes have a larger theoretical specific surface area. The difference between the theoretical and measured capacitance values that resulted from an increase in the rGOs amount may be associated with the insufficiency of electrolyte for wetting or a lack of the surface area. A thin film formed using Nafion binder covers a part of available pores, thereby blocking them [20].

Fig. 5(a-d) presents the cyclic voltammograms of CoTSPC/rGO/GC electrode composites placed in a 1 M H_2SO_4 solution obtained at a scan rate of 10 mV s^{-1}. With an increase in the phthalocyanine percentage, CoTSPC with rGO provides a wider graph and the surface area under the curve increases. This phenomenon results in an increase in the capacitance value of CoTSPC with rGO, which varies for different amounts of rGO with CoTSPC. Fig. 5 presents the cyclic voltammograms for different amounts (5, 10, 15 and 20%) of CoTSPC with GO composites with peaks obtained at various scan rates of 5, 10, 20, 30, and 40 mV s^{-1} (Fig. 6). Using these scan rates, a rectangular graph was obtained, which was slightly different from that expected for GO with phthalocyanine. This finding is well in agreement with other reports [21].

In 1 M H_2SO_4 medium, capacitance resulted from simultaneously occurring the reduction and oxidation, *i.e*., the redox reactions of functional groups present on the surface of CoTSPC molecules. In these composites, two electrons and protons are involved during redox process. The -NH group of CoTSPC molecules exhibits relatively larger capacitance. When rGO is accompanied with this functional group, the surface area of CoTSPC molecules can be increased, which increases the peak broadness and area under the curve. The -NH groups having rGO can provide broader peaks; this broadness increases with an increase in the weight percentage of CoTSPC with rGO and in with scan rate, that is, 5, 10, 20, 30 and 40 mV s^{-1}.

Kodama *et al*. [26] reported that nitrogen present in pyrrole and pyridine is highly electroactive and can increase super capacitance because -NH or nitrogen available in pyrrole-like molecules enhances GCE charge mobility due to its electron donation property and improves catalytic actions during electron transfer. With an increase in the CoTSPC with GO percentage, the peak current and area under the curve increases, indicating that the supercapacitance behaviour increases (Fig. 5).

Redox curves change with the increase in the CoTSPc with rGO concentration (Fig. 5). With an increase in the percentage

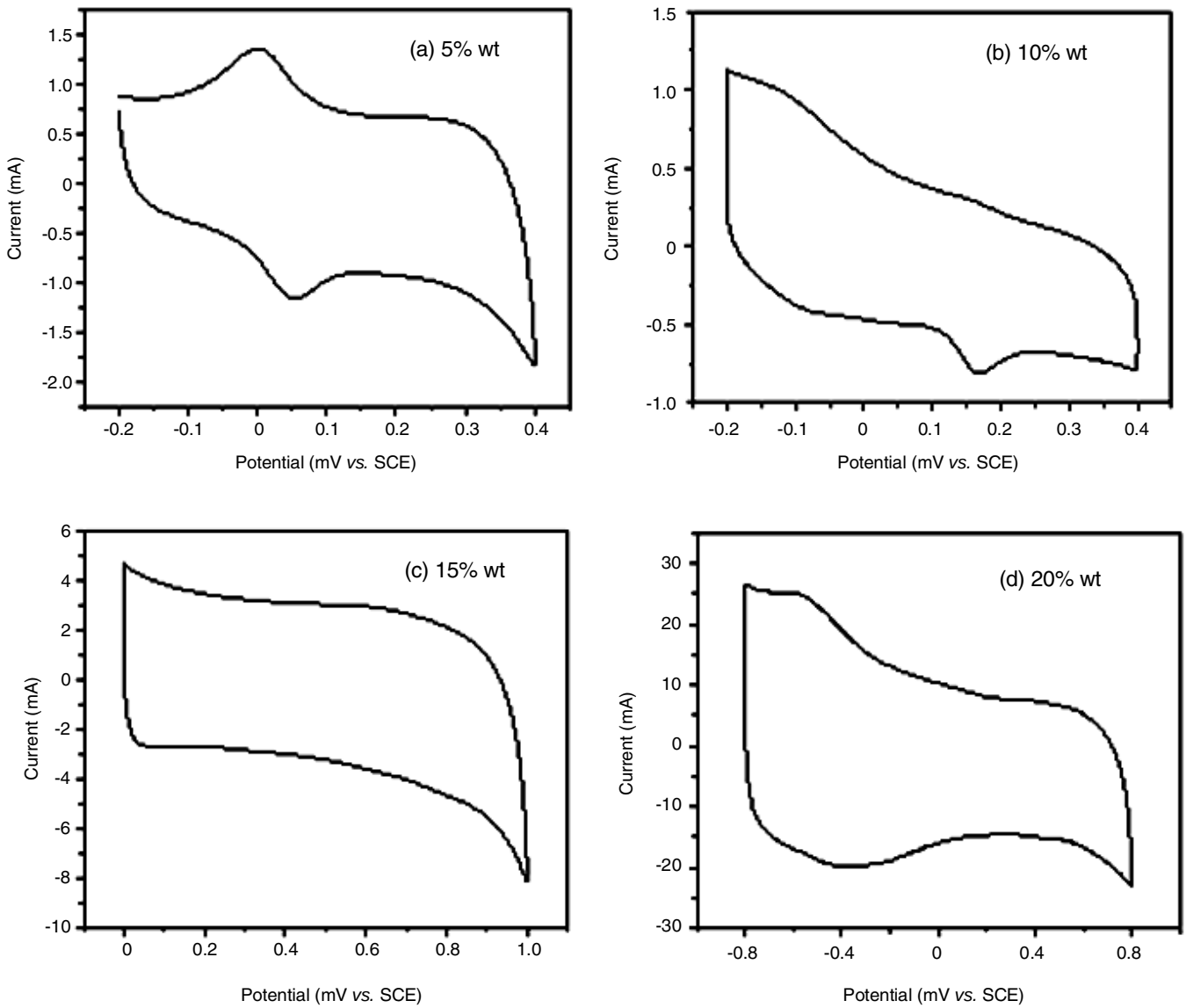

Fig. 5. Cyclic voltammetry graphs of rGO–CoTSPC composites with different weight of CoTSPC inset a to d curve, at applied scan rate of 10 mV s^{-1} in 1 M H_2SO_4 electrolyte solution

weight, the area under the curve increases. The peak current of the redox curve increased to 2 m/A for the 5% weight (Fig. 5a). For 10% weight, the peak current increased to 6.9 m/A (Fig. 5b). For 15% weight, the peak current increased to 11.2 m/A (Fig. 5c) and Fig. 5d shows an increase in the peak current to 26 m/A. The present findings confirmed that with the increase in the number of nitrogen atoms in molecules, their capacitance behaviour improves [27]. A linear plot was obtained for the scan rate versus anodic current (peak current) and cathodic current (Fig. 6a-d), which showed a surface bounding redox system. Using this linear plot, for the scan rate of 5, 10, 20, 30 and 40 mV s^{-1} were obtained, the slopes of 0.481, 0.111, 2.67 and 0.392 μM at different percentage weights (5, 10, 15 and 20% weight).

Fig. 6a presents redox curves for 5% weight of CoTSPc. The peak current increased with an increase in the scan rate from 5 to 40 mV. Thus, a graph of peak current versus different scan rates was plotted, which provided an adj. R^2 value of 0.989. When the CoTSPc weight increased from 10% to 20% weight, at various scan rates, different redox curves were observed (Fig. 6b-d). According to these graphs, corresponding linear graphs were plotted. From the new plots at different scan rates, we obtained Adj. R-square values as 0.999, 0.977 and 0.973 for 10, 15 and 20% weight of CoTSPc, respectively. Cathodic and anodic currents steadily increased with an increase in scan rates, which can be evidenced from linear graphs. The specific capacitance can be calculated by using the formula:

$$C = \frac{\int_{v_1}^{v_2} jdV}{v(v_2 - v_1)} (F/g)$$

where j is the current density (A/g), ν is scan rate (V S^{-1}) and (ν_2-ν_1) is potential window (v), the estimated capacitance values getting from CV graph with respect to scan rate.

Fig. 7 presents the estimated values of capacitance obtained from the CV graphs for different scan rates. With an increase in the scan rate, the area under the curve increases. When this

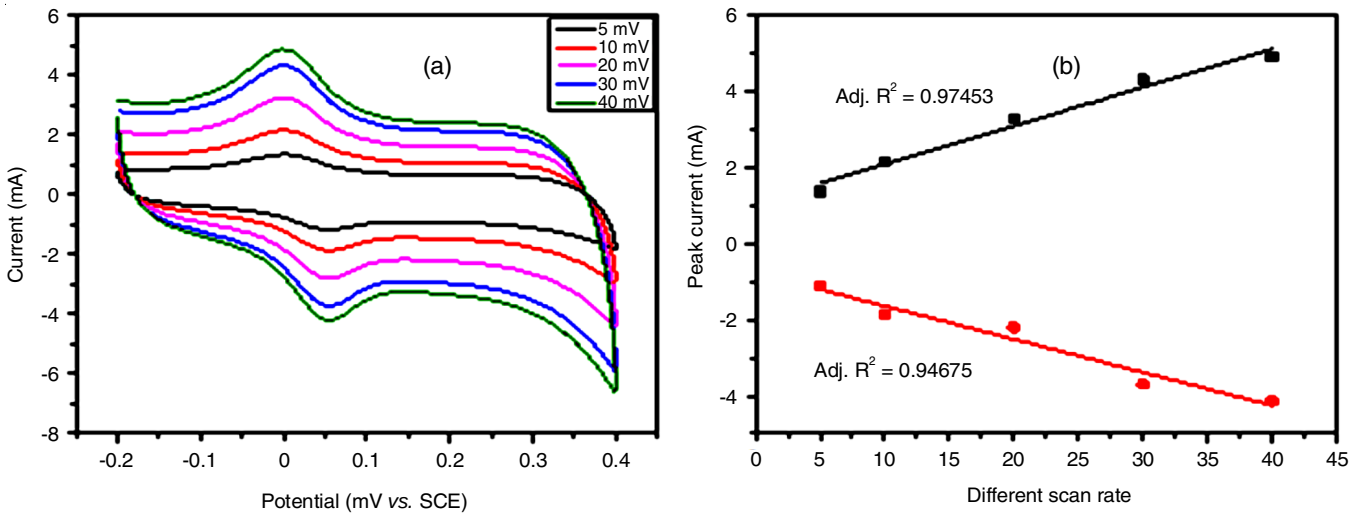

Fig. 6a. CV curves for a) different scan rate of (5% wt.) CoTSPC/rGO/GCE and b) linear plot for different scan rate *vs*. peak current, in 1 M H_2SO_4 electrolyte solution

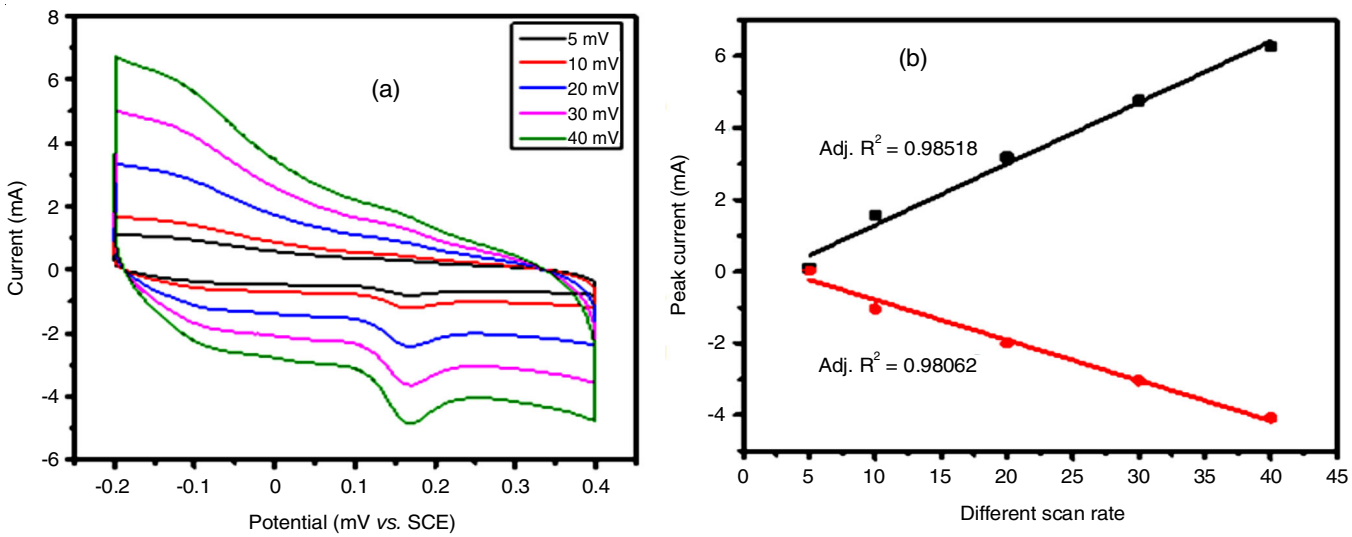

Fig. 6b. CV curves for a) for different scan rate (10% wt.) CoTSPC/rGO/GCE and b) linear plot for different scan rate *vs.* peak current, in 1 M H_2SO_4 electrolyte solution

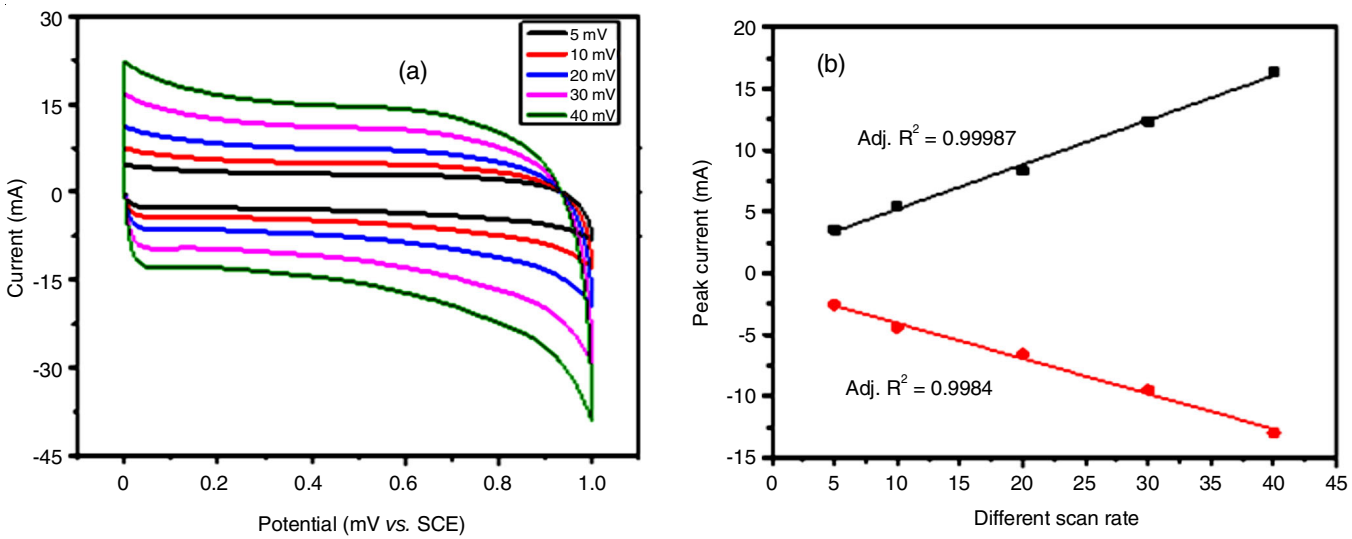

Fig. 6c. CV curves for a) different scan rate (15% wt.) CoTSPC/rGO/GCE and b) linear plot for different scan rate *vs*. peak current in 1 M H_2SO_4 electrolyte solution

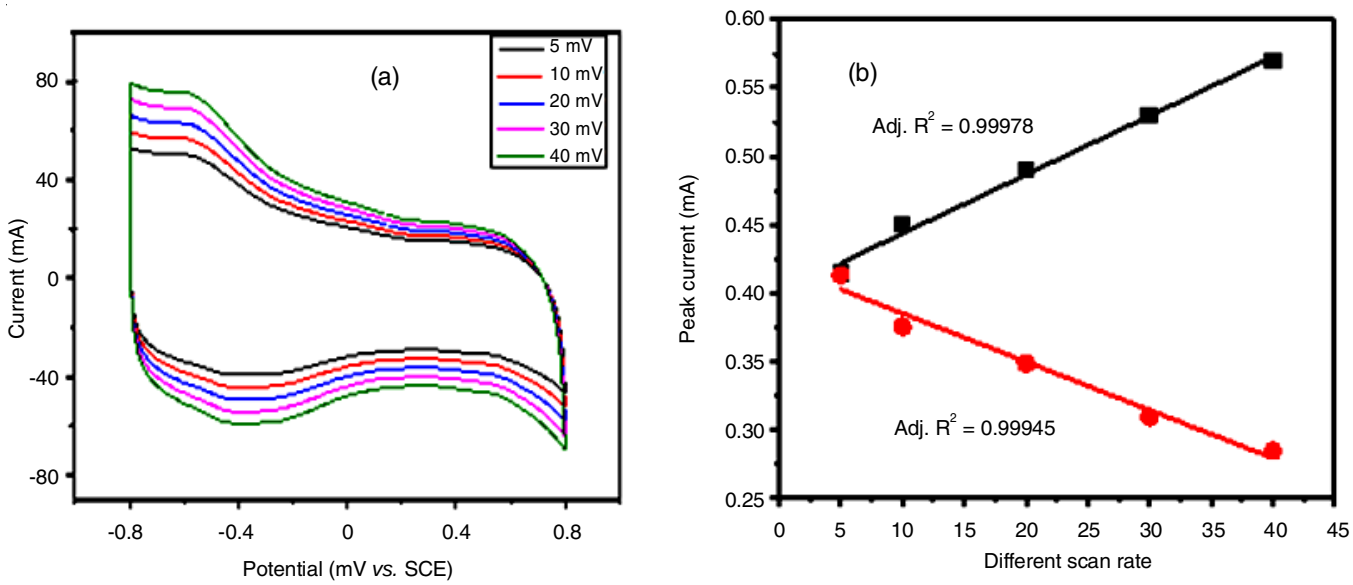

Fig. 6d. CV curves for a) different scan rate (20% wt.) of CoTSPC/rGO/GCE and b) linear plot for different scan rate *vs*. peak current in 1 M H_2SO_4 electrolyte solution

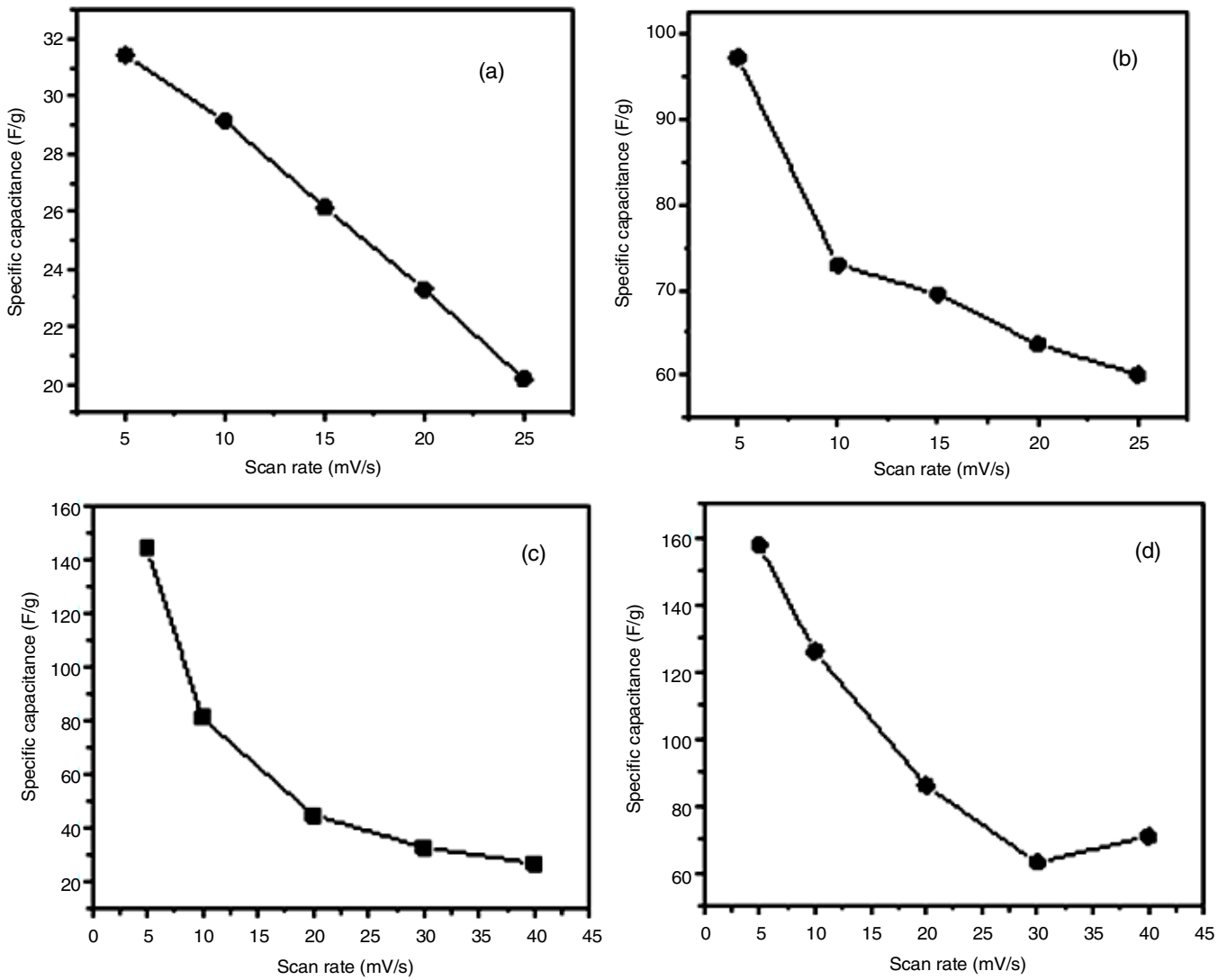

Fig. 7. Curves showing different scan rate *vs*. specific capacitance for (a) 5% wt., (b) 10% wt., (c) 15% wt. And (d) 20% wt. By CoTSPC/rGO/GCE in 1M H_2SO_4 electrolyte solution

area increases, specific capacitance decreases. The specific capacitance was highest at a lower scan rate because ions present in the electrolyte accessed the maximum surface area of electrode because of longer diffusion time [28]. Moreover, with an increase in the weight of COTSPC with GO present in the electrode material, specific capacitance increases because of an increased availability of nitrogen atoms present in the pyrrole rings of phthalocyanine [29-33].

A graph of the scan rate *versus* specific capacitance (Fig. 7) shows that a decrease in specific capacitance values led to an increase in the scan rates. A steady decrease was observed in specific capacitance values when scan rate values increase. A comparison of specific capacitance values (Fig. 7a-d) indicated that these values increase when the weight of CoTSPC with rGo increases.

Fig. 7 presents the plot of specific capacitance values *versus* scan rates. At lower scan rates, specific capacitance values were maximum and these values gradually decreased with an increase in the scan rate. Fig. 7a presents the plot for the 5% weight of CoTSPC with rGO with a capacitance of 31.42 F g^{-1} at 5 mV s^{-1}. Fig. 7b shows that for 10% weight of CoTSPc with GO the specific capacitance increased to 77.10 F g^{-1} at 5 mV s^{-1}. At 5 mV s^{-1}, the specific capacitance for 15 and 20% weight of CoTSPC was 144 (Fig. 7c) and 157 F g^{-1} (Fig. 7d), respectively. These values indicated that specific capacitance increased with the increase in the scan rate and these values increased with the weight of CoTSPc with rGO. Thus, an increase in the number of -NH in composites increases the capacitance of the composites.

Conclusion

A low-cost, simple, and environmental friendly method was developed to fabricate CoTSPC/rGO/GCE composites. The composites were prepared by increasing the rGO weight (5, 10, 15 and 20% weight) were analyzed at various scan rates (5, 10, 20 30 and 40 mV s^{-1}). The redox curve became broader when the scan rate increased, which led to an increase in the area under the curve. Positive synergistic effects caused by capacitance superimposition and double-layer capacitance enhance the specific capacitance. Furthermore, CoTSPC/rGO/GCE composites provide good recycling and excellent rates.

ACKNOWLEDGEMENTS

One of the authors, (NYPK) is grateful for the financial support by VGST (GRD No: 229), Government of Karnataka CISEE Project.

CONFLICT OF INTEREST

The authors declare that there is no conflict of interests regarding the publication of this article.

REFERENCES

1. G. de la Torre, C.G. Classens and T. Torres, *Chem. Commun.*, **20**, 2000 (2007); https://doi.org/10.1039/B614234F
2. M. García-Iglesias, J.-J. Cid, J.-H. Yum, A. Forneli, P. Vázquez, M.K. Nazeeruddin, E. Palomares, M. Grätzel and T. Torres, *Energy Environ. Sci.*, **4**, 189 (2011); https://doi.org/10.1039/C0EE00368A
3. Mounesh and K.R. Venugopala Reddy, *Anal. Chem. Lett.*, **10**, 33 (2020); https://doi.org/10.1080/22297928.2020.1745683
4. C.G. Claessens, U. Hahn and T. Torres, *Chem. Rec.*, **8**, 75 (2008); https://doi.org/10.1002/tcr.20139
5. E.-H. Liu, X.-Y. Meng, R. Ding, J.-C. Zhou and S.-T. Tan, *Mater. Lett.*, **61**, 3486 (2007); https://doi.org/10.1016/j.matlet.2006.11.091
6. A. Burke, *J. Power Sources*, **91**, 37 (2000); https://doi.org/10.1016/S0378-7753(00)00485-7
7. B.E. Conway, V. Birss and J. Wojtowicz, *J. Power Sources*, **66**, 1 (1997); https://doi.org/10.1016/S0378-7753(96)02474-3
8. Y. Ma, H. Su, X. Kuang, X. Li, T. Zhang and B. Tang, *Anal. Chem.*, **86**, 11459 (2014); https://doi.org/10.1021/ac503622n
9. G.R. Monama, M.J. Hato, K.E. Ramohlola, T.C. Maponya, S.B. Mdluli, K.M. Molapo, K.D. Modibane, E.I. Iwuoha, K. Makgopa and M.D. Teffu, *Results Physics*, **15**, 102564 (2019); https://doi.org/10.1016/j.rinp.2019.102564
10. Z. Xu, Z. Li, C.M.B. Holt, X. Tan, B.S. Amirkhiz, T. Stephenson, H. Wang and D. Mitlin, *J. Phys. Chem. Lett.*, **3**, 2928 (2012); https://doi.org/10.1021/jz301207g
11. M. Soylu, R. Ocaya, H. Tuncer, A.A. Al-Ghamdi, A. Dere, D.C. Sari and F. Yakuphanoglu, *Microelectr. Eng.*, **154**, 53 (2016); https://doi.org/10.1016/j.mee.2016.01.022
12. P.M. Mounesh, P. Malathesh, N.Y. Praveen Kumara, B.S. Jilani, C.D. Mruthyunjayachari and K.R. Venugopala Reddy, *Heliyon*, **5**, e01946 (2019); https://doi.org/10.1016/j.heliyon.2019.e01946
13. K.R. Mounesh and K.R. Venugopal Reddy, *New J. Chem.*, **44**, 3330 (2020); https://doi.org/10.1039/C9NJ05807A
14. B. Chidananda, K.R. Venugopala Reddy, M.N.K. Harish, K.M. Pradeep, C.D. Mruthyunjayachari and S.D. Ganesh, *J. Heterocycl. Chem.*, **52**, 1782 (2014).
15. K.R. Mounesh and K.R. Venugopala Reddy, *Anal. Chim. Acta*, **1108**, 98 (2020); https://doi.org/10.1016/j.aca.2020.02.057
16. X. Zhang, Y. Feng, S. Tang and W. Feng, *Carbon*, **48**, 211 (2010); https://doi.org/10.1016/j.carbon.2009.09.007
17. K.P. Madhuri and N.S. John, *Appl. Surf. Sci.*, **449**, 528 (2017); https://doi.org/10.1016/j.apsusc.2017.12.021
18. L. Ding, Z. Wang, Y. Li, Y. Du, H. Liu and Y. Guo, *Mater. Lett.*, **74**, 111 (2012); https://doi.org/10.1016/j.matlet.2012.01.070
19. B.S. Mounesh, B.S. Jilani, M. Pari, K.R.V. Reddy and K.S. Lokesh, *Microchem. J.*, **147**, 755 (2019); https://doi.org/10.1016/j.microc.2019.03.090
20. N. Blomquist, T. Wells, B. Andres, J. Bäckström, S. Forsberg and H. Olin, *Sci. Rep.*, **7**, 39836 (2017); https://doi.org/10.1038/srep39836
21. F. Béguin, V. Presser, A. Balducci and E. Frackowiak, *Adv. Mater.*, **26**, 2219 (2014); https://doi.org/10.1002/adma.201304137
22. B.N. Achar, T.M. Mohan Kumar and K.S. Lokesh, *J. Coord. Chem.*, **60**, 1833 (2007); https://doi.org/10.1080/00958970701194090
23. K.S. Lokesh and A. Adriaens, *Dyes Pigments*, **96**, 269 (2013); https://doi.org/10.1016/j.dyepig.2012.08.018
24. K.S. Lokesh, N. Uma and B.N. Achar, *Polyhedron*, **28**, 1022 (2009); https://doi.org/10.1016/j.poly.2009.01.034
25. W. Xing, S.Z. Qiao, R.G. Ding, F. Li, G.Q. Lu, Z.F. Yan and H.M. Cheng, *Carbon*, **44**, 216 (2006); https://doi.org/10.1016/j.carbon.2005.07.029
26. D. Hulicova-Jurcakova, M. Kodama, S. Shiraishi, H. Hatori, Z.H. Zhu and G.Q. Lu, *Adv. Funct. Mater.*, **19**, 1800 (2009); https://doi.org/10.1002/adfm.200801100
27. J.N. Lekitima, K.I. Ozoemena and N. Kobayashi, *ECS Trans.*, **50**, 125 (2013); https://doi.org/10.1149/05043.0125ecst
28. M. Samanta, P. Howli, U.K. Ghorai, M. Mukherjee, C. Bose and K.K. Chattopadhyay, *Physica E*, **114**, 113654 (2019); https://doi.org/10.1016/j.physe.2019.113654

29. P. Gong, Y.-J. Li, Y.-H. Jia, Y.-L. Li, S.-L. Li, X.-Y. Fang and M.-S. Cao, *Phys. Lett. A*, **382**, 2484 (2018); https://doi.org/10.1016/j.physleta.2018.06.006
30. Y.-J. Li, S.-L. Li, P. Gong, Y.-L. Li, X.-Y. Fang, Y.-H. Jia and M.-S. Cao, *Physica E*, **104**, 247 (2018); https://doi.org/10.1016/j.physe.2018.08.001
31. Y.-J. Li, S.-L. Li, P. Gong, Y.-L. Li, X.-Y. Fang, Y.-H. Jia and M.-S. Cao, *Physica B*, **539**, 72 (2018); https://doi.org/10.1016/j.physb.2018.04.004
32. G. Wang, G. Yang, Z. Chen, J. Liu, X. Fan, P. Liang, Y. Huang, J. Lin and Z. Shen, *J. Power Sources*, **419**, 82 (2019); https://doi.org/10.1016/j.jpowsour.2019.02.029
33. N. Senthilkumar, V. Venkatachalam, M. Kandiban, P. Vigneshwaran, R. Jayavel and I.V. Potheher, *Physica E*, **106**, 121 (2019); https://doi.org/10.1016/j.physe.2018.10.027